Development of optical imaging system for LIGO test mass contamination and beam position monitoring

Chen Jie Xin [1]
Mentors: Keita Kawabe, Rick Savage, Dan Moraru [2]
23 Septermber 2016

Abstract

Optical losses due to large angle scattering from test masses at the ends of the LIGO interferometer arms can be monitored using an existing camera system using DSLR cameras with telephoto lens. This project aims to calibrate the system and to install a similar system—using a telescope instead of telephoto lens—for monitoring the corner station test masses. For calibration, the relation between the pixel values and the number of photons incident on the camera was investigated by shining a laser at various power settings onto the camera sensor. The relationship between actual shutter speed and nominal shutter speed was also investigated by photographing a DC light source. Finally optical losses through the camera lens and telescope was also investigated. Further work to determine the losses through the viewport is necessary for full calibration. For the corner station camera system, a custom remote focusing system—consisting of a PLC program and GUI—was developed. Currently, the system supports position readout and jog control, and support for position presets and position control is under development. Further work consists of physical installation of the camera system and integration of the remote focusing program into existing infrastructure. Software and consolidated data sets can be found in the document `LIGO-T1600390-v1` on the LIGO DCC.

Introduction

The LIGO interferometer is a modified Michelson interferometer with two orthogonal, 4-kilometer long "arms" [1]. For each arm there are two test masses—both 40 kg mirrors; one is at the end of the arm (the end test mass) and the other (the input test mass) is at the corner station, where the two arms meet [1]. This forms a 4 km long Fabry-Pérot cavity, within which the input laser light travels back and forth multiple times [2].

The circulation of light in the cavity multiplies the power of the input beam and the distance travelled by the beam to achieve the sensitivity necessary to detect the small length fluctuations due to gravitational waves [2]. Therefore, it is desirable to maintain low optical losses in these resonators [3].

Understanding the optical performance of the test mass mirrors in the operating interferometer could provide the basis for improvements in the performance of the optics and, consequently, the sensitivity of the interferometer [4]. Observing the light scattered from test masses with a camera system can contribute to understanding their performance.

Project Scope

Presently, cameras for observing the end test masses have already been installed and are operational. These cameras are part of the photon calibrator (PCAL) beam localisation camera systems and are used to determine the location of the PCAL beams on the ETM surfaces [5].

However, in addition to monitoring PCAL beam positions on the test masses, the camera system can also be used to capture images of the test masses when either 532 nm or 1064 nm laser light

[1] LIGO SURF Program, Summer 2016
[2] LIGO Hanford Observatory

is resonating in the arms of the interferometer. These images provide a qualitative picture of light scattered from the test masses, but a quantitative estimate of the power loss due to the scattering yet to be made. Since the scattering is thought to most likely be due to the combination of the internal imperfections of the reflective coating, as well as particulate contamination of the test masses surfaces, obtaining a quantitative estimate can help in understanding the amount of the additional optical losses introduced by the contamination at the end test masses. To do so, the camera system needs to be calibrated.

Moreover, as the camera system was originally intended for PCAL beam localisation at the end test masses, they have yet to be installed at the input test masses. However, unlike the end test mass camera system, the input test mass camera system uses a Celestron 8" EdgeHD Schmidt-Cassgrain telescope instead of a telephoto zoom lens. This is because the viewports for the input test masses are several times further away—at a distance of 32.756 m [6]—from the test mass surface than those for the end test masses.

While the focus and zoom of the telephoto lens at the end test mass camera system can be controlled directly through the same Nikon Camera Control Pro 2 software used for capturing the images, the Celestron telescope requires an external controller connected to a focuser to adjust zoom and focus. For integration into the existing slow controls systems, a Beckhoff EP7041-2002 fieldbus module is used, in conjunction with a MoonLite high resolution stepper motor and focuser. A user interface for operators in the control to adjust the focus of the camera also needs to be developed.

Methods

Camera Calibration Overview

In order to determine the power of the scattered light from the camera images, the pixel values of the camera images must be related to the amount of power incident on the camera sensor. Using the power incident on the camera sensor, and the amount of transmission losses when the scattered light passes through the viewport and the lens to the camera sensor, the original power of the scattered light can be determined. So, we have

$$P_o = T_{\text{viewport}}\, T_{\text{lens}}\, P_i\,(\text{pixel values}, \text{camera settings})$$

where P_o and P_i are respectively the power of the light incident on the viewport, and the power of the light incident on the camera, and T are the transmissivities of the viewport and lens. The scope of this project is to determine the transmissitivities of the lens that are, or will be, used in the camera system, and determine function that maps pixel values and camera settings to the power P_i incident on the camera sensor for 1064 nm laser light.

Lens Calibration

To determine the transmissivity of the lens, the laser of known wavelength was shone through the lens, and the power of the laser beam before and after lens was measured. The transmissivity was calculated by taking the ratio between the power after and the power before. The laser used was a 1064 nm OZOptics fiber coupled laser, and the lens calibrated were the AF-S DX Nikkor 55–300 mm f/4.5–5.6G ED VR and Tamron SP 150–600 mm f/5–6.3 Di VC USD telephoto lens, and the Celestron 8" EdgeHD Schmidt-Cassegrain telescope. The Tamron lens are intended to replace the Nikkor lens at the end test masses [6], while the Celestron telescope will be used for the input test mass camera system.

The telephoto lens, kept at maximum aperture by taping down the aperture lever, were mounted on an optical table and the laser was aligned such that it passed through the center of the lens surface to ensure that the beam was not clipped by the edges of the lens. The telescope was also mounted in a similar fashion, but aligned so that the beam was not clipped by the secondary mirror inside the telescope. To ensure that the beam was not clipped, the alignment was checked using an infrared viewer and a sensor card.

Finally, an Ophir Nova power meter with photodiode sensors was used to measure the input power, and then moved to the other side of the lens to measure the output power. The full set-up is as in Fig. 1.

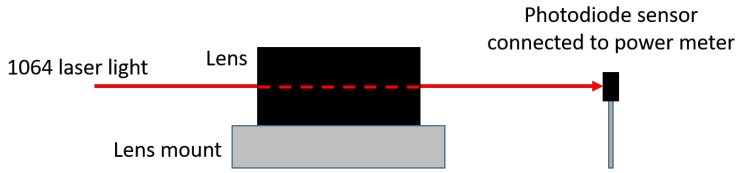

Figure 1: Set-up for measuring lens transmissivity

Camera Sensor Calibration

The camera sensor was calibrated using the same 1064 nm OZOptics fiber coupled laser shining directly on the camera's sensor. This was accomplished by removing the camera lens, so sensor is exposed directly to the laser when the shutter is open. The camera was mounted on a tripod at the edge of the optical table. The power of the laser beam was changed by adjusting the power input to the laser, and the power of the beam incident on the camera sensor was measured with a an Ophir Nova power meter connected to a photodiode sensor placed directly in front of the camera. Images were then taken at that particular power at different camera settings. The set up the camera sensor calibration is pictured in Fig. 2. For each camera setting, "dark" frames with the

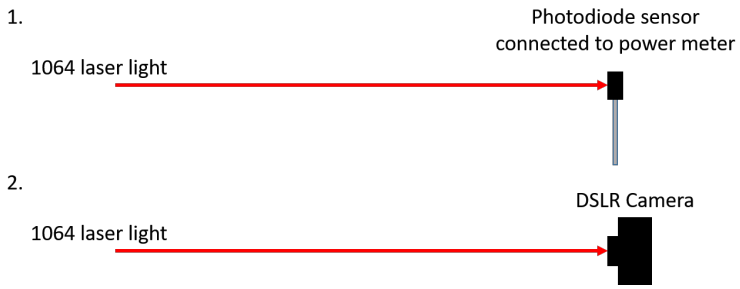

Figure 2: Set-up for measuring camera sensor response. 1. Measure power of laser light using photodiode sensor connected to power meter. 2. Take images of the beam using DSLR camera.

beam path blocked were taken at the beginning of the measurement, followed by "bright" frames with the beam path unblocked.

For the first round of data collection, we used a narrow beam directly incident on the camera sensor. We verified that the beam was not clipped visually using LiveView on the camera, and also

ensured that the images we took were not saturated by monitoring the pixel value histogram on the camera display. Images were taken at various ISO setting with exposure time of 1/2500 s for power ranging from 114 μW to 370 μW.

A second round of data collection was conducted using a wider beam profile by placing a biconcave lens between the beam and the camera. Images were taken at ISO 100 for power ranging from 250 μW to 1380 μW. ISO 100 was used since it was the setting at which most of the images of test masses are being taken at.

For each power and camera setting, multiple "dark" and "bright" frames were taken and saved in uncompressed 14-bit colour depth NEF format. The NEF format is Nikon's proprietary RAW image format, which purportedly retains unprocessed camera sensor pixel data [7]. The format is readable using `rawpy` a Python wrapper for raw image reader `dcraw`. The extracted image data is a 6036 $\times$ 4020 (corresponding to the dimensions of the image) containing pixel values, which range from 0 to $2^{14} - 1$. Each "pixel" in the matrix is also associated with a colour—red, green, or blue—which is colour of the part of the Bayer colour filter array (Fig. 3) overlaying the pixel [8]. The colour information can also be extracted from the RAW image as a 6036 $\times$ 4020 matrix.

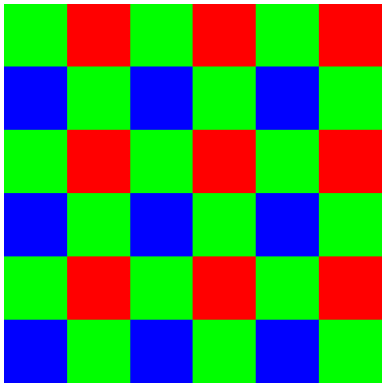

Figure 3: Bayer colour filter arrays in camera sensors used to produce colour images by interpolating pixel values of adjacent coloured pixels. As seen from the image, there is an equal amount of red and blue pixels, and twice as many green pixels.

Finally, flat frames illuminated by a single red LED connected to a DC source were taken using the Nikon DSLR Camera at different shutter speeds to determine whether pixel values varied linearly with shutter speed. Linearity with shutter speed would be desirable since that would allow us to normalise images taking at different shutter speeds by dividing counts by the length of exposure.

Input Test Mass Camera System

Developing the input test mass camera system consists of determining how to interface our chosen MoonLite high resolution stepper motor and focuser with the EP7041 Beckhoff stepper motor controller module, and programming the Beckhoff module using the TwinCAT 2 software provided by Beckhoff. Programming and testing took place on a test stand separate from the main Beckhoff controls.

Furthermore, we also set up the camera system on a tripod at the viewport at the corner station to test the quality and resolution of the images of the test masses using the system. Physical

installation of the camera system did not actually take place before the conclusion of this project, because the housing for the camera and telescope were found to not have enough clearance from the beam tube.

Findings and Results

Lens Calibration

The transmissivity T of the lens were calibrated by measuring the power of the beam entering the lens, and the power of the beam exiting the other side of the lens using a power meter. The transmissivity is calculated using the equation

$$T = \frac{P_{\text{out}}}{P_{\text{in}}} \times 100\%$$

where P_{in} and P_{out} are the power entering and exiting the lens, respectively. The power measurements are as follows:

Lens	P_{in}/mW	P_{out}/mW	T/%
Nikkor 55–300 mm lens	9.8 ± 0.01	1.95 ± 0.01	19.8 ± 0.1
Tamron SP 150–600 mm lens	8.27 ± 0.01	1.15 ± 0.01	13.9 ± 0.1
Celestron 8" EdgeHD telescope	8.29 ± 0.01	2.81 ± 0.01	33.9 ± 0.2

Table 1: Lens transmissivity measurements

As seen from the data, losses will be greatest (i.e. lowest transmissivity) through the Tamron lens, and lowest through the Celestron telescope.

Camera Sensor Calibration

In the analysis of NEF format images from the Nikon DSLR camera, all the pixels of the same colour were assumed to be identical, and we summed over all the pixel values for each colour for every image to get the total colour pixel value. For each set of images, we took the mean of the total colour pixel values of the set to obtain the average total colour pixel values for that set. The average total pixel values were then plotted against the appropriate independent variables.

For the shutter speed measurements, measurements were taken for exposure times up to 0.5 s at ISO 640 such that even the lowest images are not completely dark. Two sample images are shown in Fig. 4. the average total pixel values were plotted against exposure time, as in Fig. 5.

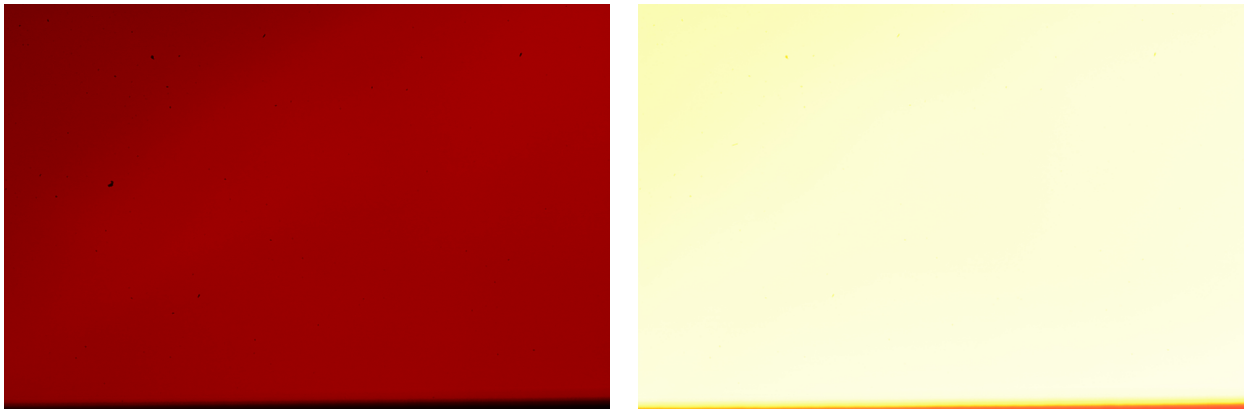

Figure 4: Left: 1/2500/,s exposure. Right: 1/2/,s

The average total pixel counts for each colour channel and each set of exposure times were plotted against exposure time to determine if counts were linear with respect to exposure time. Each colour channel only had useful data for exposure times up to the point where the particular channel started saturating; since we used a red LED, the red channel saturated very early, followed by the green channel. The blue channel, however, did not saturate for the entire range of shutter speeds tested, and so is given in Fig. 5.

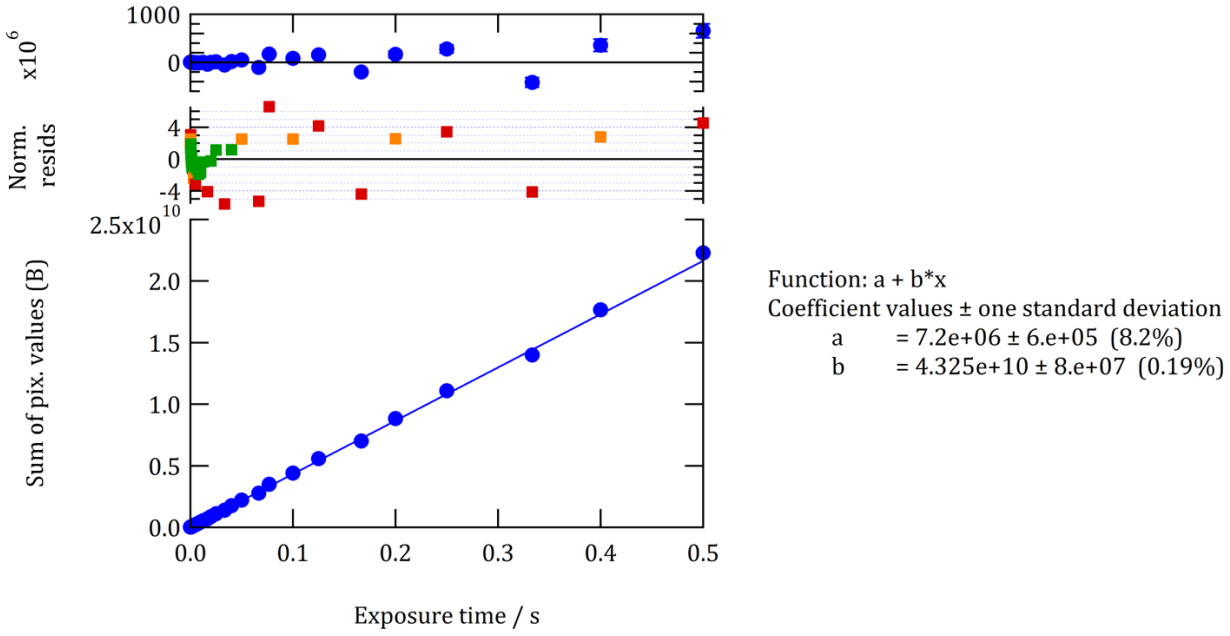

Figure 5: Plot of average total pixel count for the blue channel against exposure time

As we can see, the pixel count does indeed appear to be linear with respect to exposure time.

Now, for the actual calibration for the laser power, two different beam profiles were used: the narrow beam and the wide beam (Fig. 6).

Figure 6: Left: Narrow beam at 1/2500 s exposure. Right: Wide beam at 1/2000 s exposure.

The resulting plots against power for images taken at 1/2500 s and 1/2000 s exposures at ISO 100 are given in Fig.7 and Fig. 8 respectively.

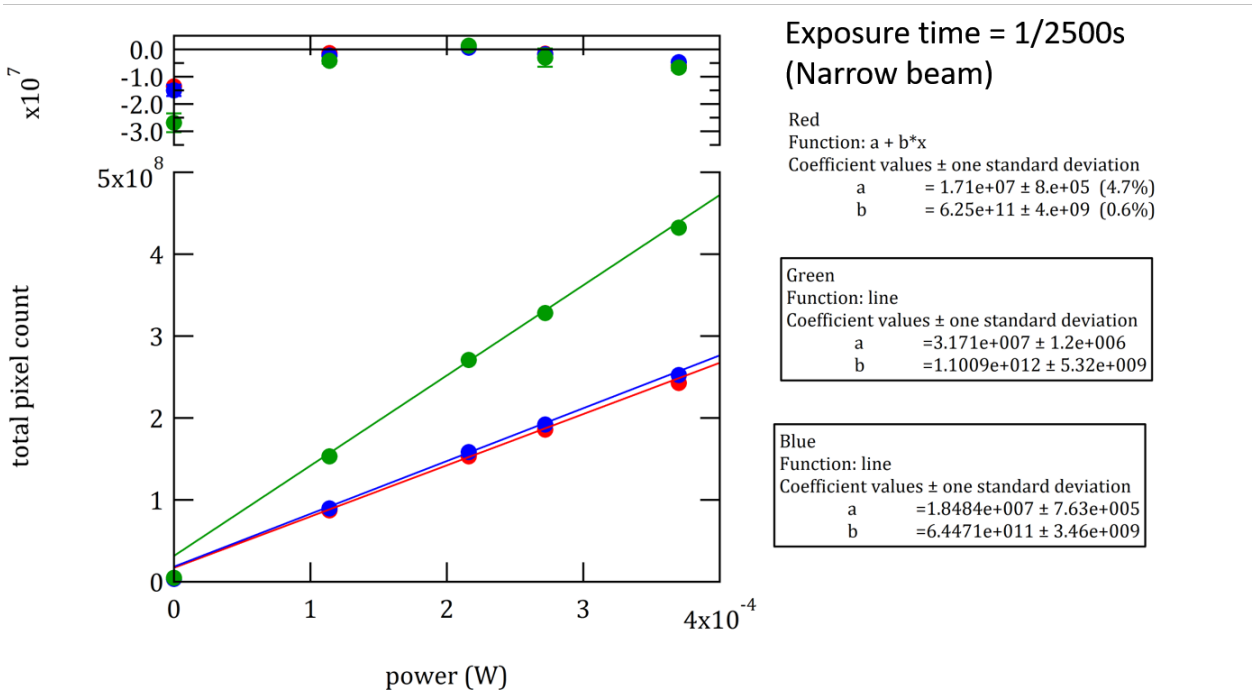

Figure 7: Plot for images taken with at 1/2500 s exposure and ISO 100. All images are taken with the narrow beam profile.

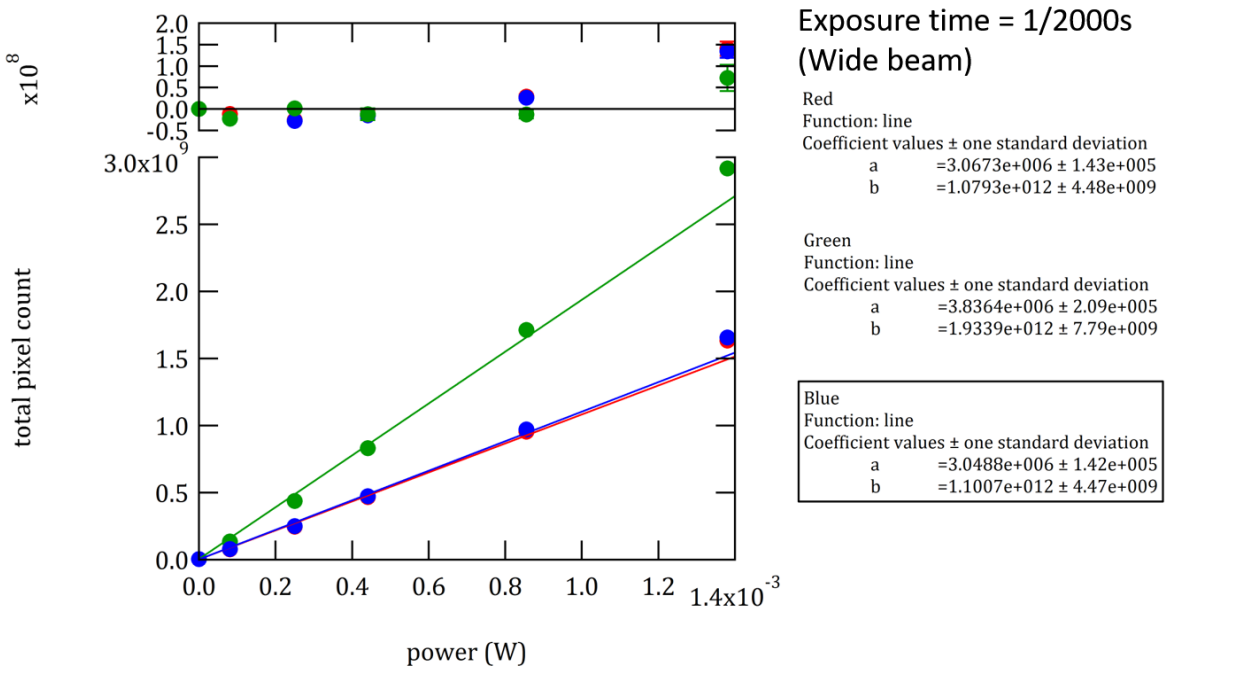

Figure 8: Plot for images taken with at 1/2000 s exposure and ISO 100. All images are taken with the wide beam profile, except the point at 81 μW, which was taken at 1/2000 s exposure with a narrow beam. The point at 81 μW was excluded from the least-squares fit.

A least-squares fit was performed for each colour channel for each data set, and the slope of the linear fit (coefficient value b) is the response of the camera sensor to power for each exposure time setting. The point at 0 is the total pixel count of the "dark" frames—while they appear to be at the origin in the plots, they are actually non-zero, but are extremely tiny compared to the counts in image with the laser beam. Hence, we can basically ignore the "dark" count in our data—which includes ambient light and the camera sensor's own dark count rate.

Now, we note that since pixel count is linear with respect to exposure time, we would expect the sensitivity at 1/2000 s exposure to to be 1.25 times higher than the sensitivity at 1/2500 s exposure. So the ratio of the slopes of the linear fits for each colour channel for 1/2000 s to that of the corresponding channel for 1/2500 s ought to be 1.25. However, comparing we have:

Colour	1/2000 s, wide beam slope/counts per watt	1/2500 s, narrow beam slope/counts per watt	Ratio
Red	1.08×10^{12}	6.05×10^{11}	1.73
Green	1.92×10^{12}	1.10×10^{12}	1.75
Blue	1.10×10^{12}	6.45×10^{11}	1.71

Table 2: Ratio of camera sensor sensitivity (slope of plots) for 1/2000 s and 1/2500 s

As seen above, the ratio of roughly 1.7 is higher than the expected 1.25. Since we know pixel values vary linearly with exposure time, the different beam profiles seem to also be affecting the camera sensitivity. It is unclear how it could be affecting the counts, though, since the pixel counts ought to only depend on the power incident on it, and not the shape of the beam. Since there

seems to be some dependence of the camera sensitivity on the beam profile, the calibrations are probably not very applicable to actual images of the test masses, since the profiles of the scattering is very different from the laser beams used in the laboratory. Thus, more work is probably needed to attain a satisfactory calibration of the camera sensor.

Input Test Mass Camera System

The cabling for the stepper motor and the Beckhoff module were determined to be as follows: The Beckhoff module requires a 24 V power supply fed through a female M8 connector, and ethernet cable through an M8 plug, and a 12 V supply for the stepper motor through female M12 5-pin connector. The stepper motor is connected to Beckhoff module with a male M12 5-pin connector to female 9-pin D-Sub connector cable wired as in Fig. 9.

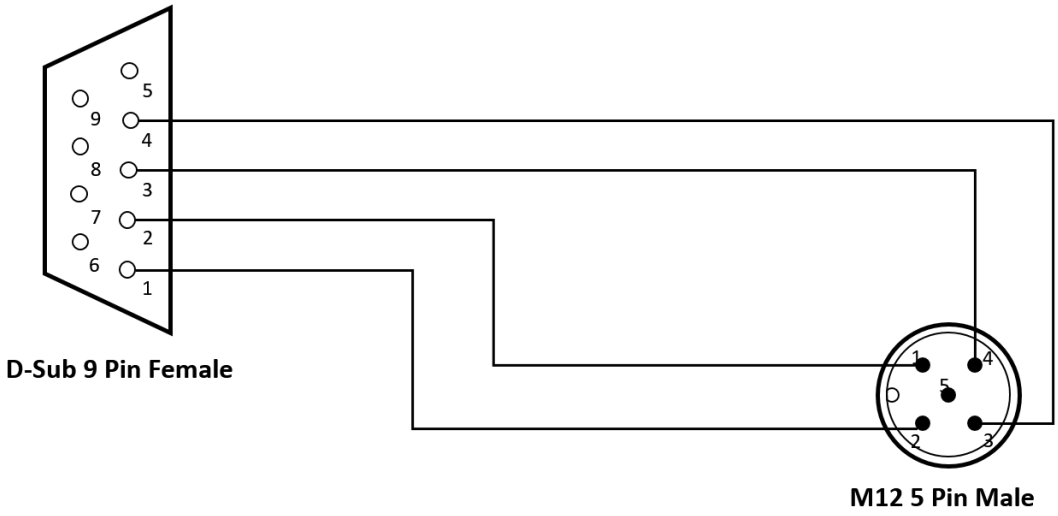

Figure 9: Pin-out for cable connecting stepper motor and Beckhoff module

The Beckhoff module is connected to the test stand via the ethernet cable, and can be configured and programmed through the TwinCAT 2 software by Beckhoff. STM settings and STM features have to be configured for the stepper motor to be usable. The main STM settings that need to be configured are nominal voltage in millivolts the maximal current in milliamperes. The stepper motor included in the MoonLite focuser and stepper motor is an LSG35012F76P Hurst unipolar motor [9], which takes a 4.5 V power and 12 V voltage [10]. Therefore, the nominal voltage setting should be set to 12000 and the maximal current should be set to 375. The full settings configuration is found in Fig. 10.

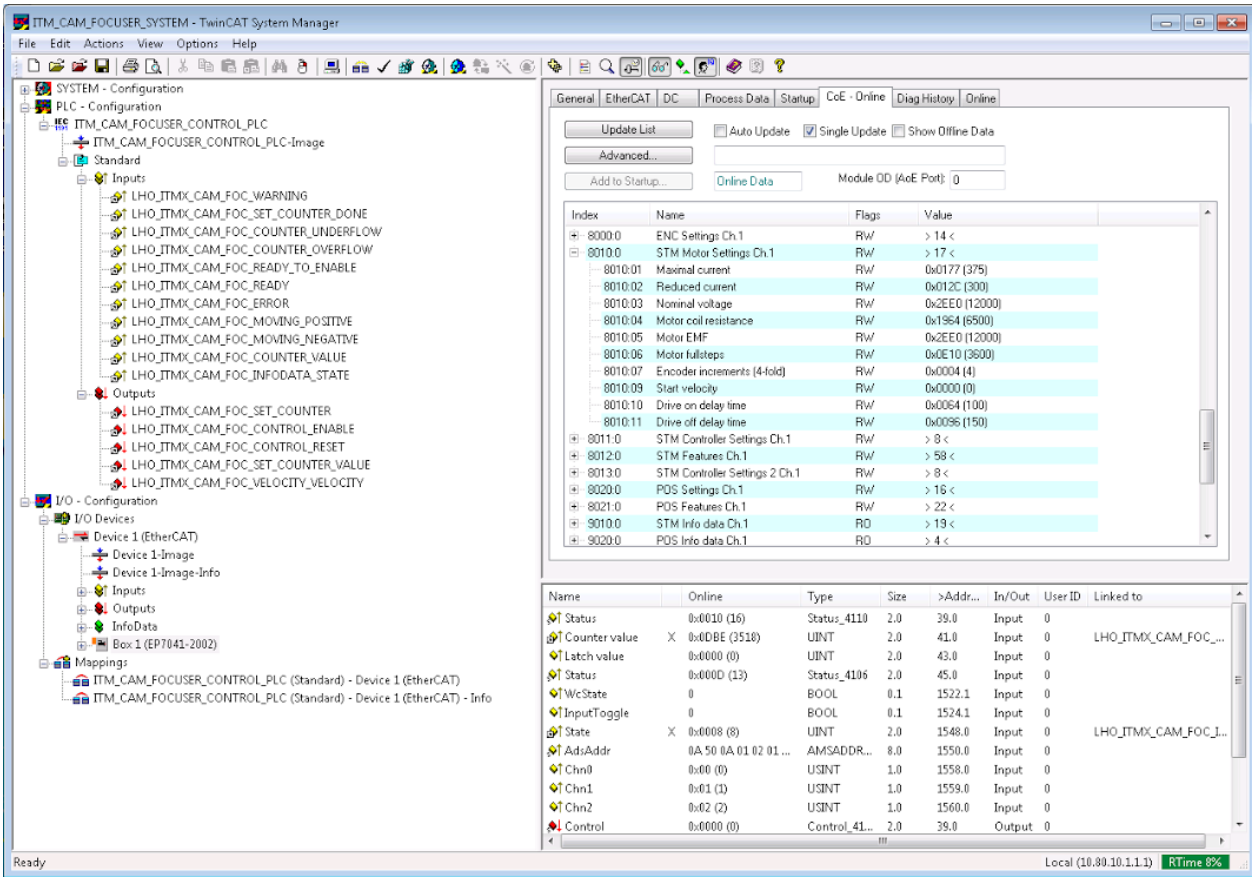

Figure 10: STM Settings configuration

For the STM features, the operation mode needs to be set to velocity direct, as that seems to be the only operation mode that is supported, and for the focuser to operate as desired, the speed range is best set to 1000 Fullsteps/sec. As we are not using an external encoder to track the position of the stepper motor, we set feedback type to internal counter. The full STM features configuration is found in Fig. 11.

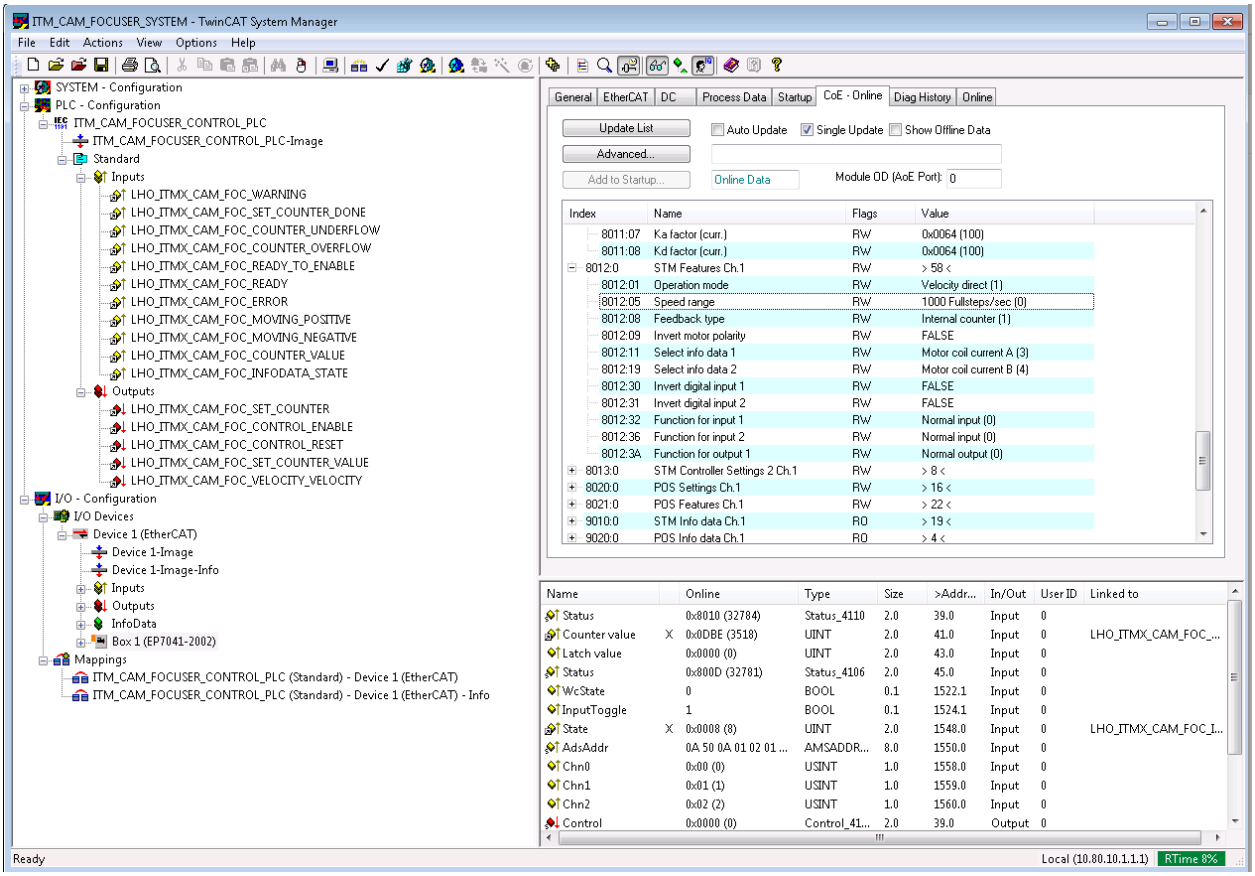

Figure 11: STM Features configuration

A PLC program was written to toggle the focuser stepper motor remotely, and graphical user interface written in MEDM so that the focuser can be jogged remotely from a computer. The interface also supports displaying and resetting the current value to arbitrary values (e.g. zero, midpoint) of the internal counter, so that users have a sense of how much the focuser has been adjusted. (Fig. 12). The for the PLC program, MEDM screen, and overall ITM configuration can be found in the same DCC document as this report (`LIGO-T1600390-v1`).

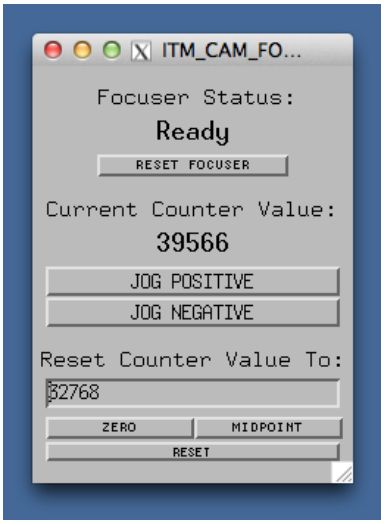

Figure 12: Prototype MEDM screen for remote control of ITM cameras

In addition to the programming the stepper motor and developing a user interface for it, we also took several test images of the input test masses at the corner stations by mounting the telescope and camera on the a tripod and manually focusing. We were able to obtain images of the ITM when both the infrared light and green 532 nm light (Fig. 13) were resonating.

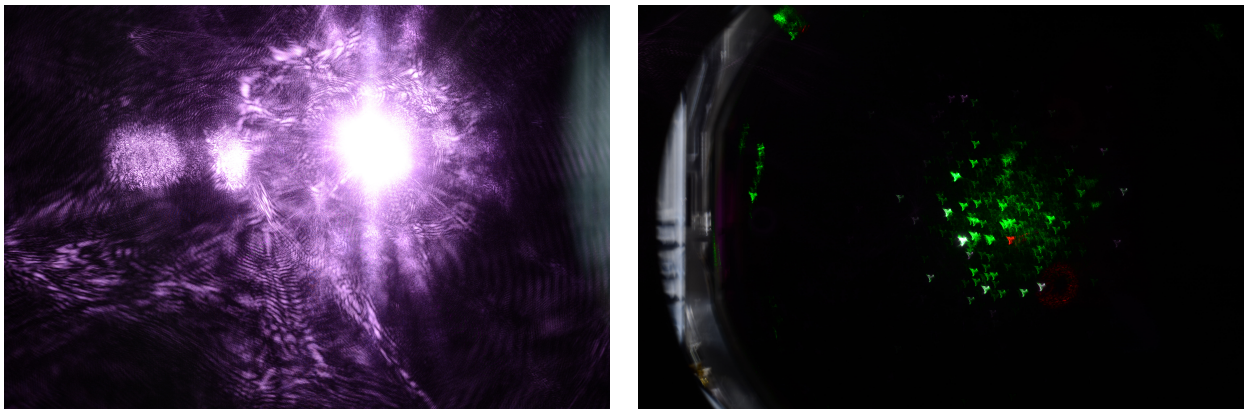

Figure 13: Left: Image of ITM with infrared light resonating taken at ISO 100 with 1 s exposure time. Right: Image of ITM with green light resonating taken at ISO 100 with 2 s exposure time.

From the image of the focused green light, there are some clear triangular artifacts in the image of the ITM. It is unclear what the origin of these distortions are, and they will have to be accounted for when the camera system is actually being put to use. It is suspected that they might be due to distortions caused by the viewport, which is only guaranteed to be flat up to a diameter smaller than the 8" telescope aperture. Other than the distortions, the telescope seems to give a rather high magnification, as the ITM appears to be filling the entire frame of the image.

Recommendations for Further Work

While the lens calibrations appear to be fairly decent, the camera calibration was not very conclusive since the sensitivity of the camera sensor differed significantly when the beam profile was changed, even when the different exposure times were adjusted for. Since the profile of the scattered light from the test mass will be very different from the beam profiles that are used in the lab for calibration, it is unclear whether this set of calibration data can be applied to actual images of the test masses.

However, we do know from the camera calibration efforts that pixel values vary linearly with exposure time, and this can serve as basis for further calibration efforts. Further work to determine whether beam profile really affects the response to the camera sensor, and why it affects the camera sensor response (when, by all accounts, it should not) ought to be conducted. Perhaps calibration measurements can be repeated with a source with variable beam width and a photodiode sensor with larger effective area to measure light with different beam profiles more effectively.

As for the input test mass camera system, further work on the program to enable direct position control, so that the user can specify the position for the focuser to move to directly is desirable. The counter for the focuser position also overflows, when it reaches the maximum or minimum counter values; this issue would probably have to be addressed in order to implement the aforementioned control. Installation of both the software and hardware is also pending.

Finally, work to understand the origins of the artifacts in the ITM images would also be desirable, in order to determine if any modifications can be made to the current planned set-up to improve the quality of the images. Strategies to explore include reducing the telescope aperture such that it collects less of the distorted light from the edges of the viewport—such an approach would probably reduce the resolution of the image, but improve the quality of the image.

References

[1] B. P. Abott, *et al.*, GW150914: The Advanced LIGO detectors in the era of first discoveries, Physical Review Letters, **116**, 131103 (2016).

[2] *LIGO's Interferometer*, WWW Document, (`https://www.ligo.caltech.edu/page/ligos-ifo`)

[3] LIGO SURF Project Proposals 2016 (Unpublished).

[4] R. Savage (private communication).

[5] D. Tuyenbayev, V. Quetschke, & R. Savage, Image analysis for the PCAL beam localization system, LIGO Document Control Center, (`https://dcc.ligo.org/LIGO-T1400543`).

[6] T. Abbott, S. Karki, R. Savage, & N. Kijbunchoo, Photon calibrator beam localization camera system description and configuration procedures, LIGO Document Control Center, (`https://dcc.ligo.org/LIGO-T1400551`).

[7] Nikon Electronic Format (NEF) From Nikon, WWW Document, (`http://www.nikonusa.com/en/learn-and-explore/article/ftlzi4ri/nikon-electronic-format-nef.html`).

[8] Digital Camera Sensors, WWW Document, (`http://www.cambridgeincolour.com/tutorials/camera-sensors.htm`).

[9] High Res Stepper Motor Combo 2015, WWW Document, (`https://focuser.com/media/Downloads/MoonLite_Software/High\%20Res\%20Stepper\%20Motor\%20Combo\%202015.docx`).

[10] LSG35 35mm Geared Permanent Magnet DC Stepper Motors, WWW Document, (`http://www.hurst-motors.com/lsg35geared.html`).